JOURNAL OF GEOPHYSICAL RESEARCH, VOL. 113, B09312, doi:10.1029/2007JB005412, 2008

Inner-core fine-scale structure from scattered waves recorded by LASA

Zhigang Peng,[1] Keith D. Koper,[2] John E. Vidale,[3] Felipe Leyton,[4] and Peter Shearer[5]

Received 30 September 2007; revised 10 April 2008; accepted 7 July 2008; published 20 September 2008.

[1] Recent observations of inner-core scattering (ICS) waves provide evidence that the outermost 300 km of the inner-core has strong heterogeneities with a length scale of a few kilometers. These waves follow a path similar to that of the inner-core–reflected waves *PKiKP* and were originally observed in data from 16 events in the distance range 58° to 73° recorded by the Large Aperture Seismic Array (LASA). Here we present additional observations of the ICS waves from a total of 78 events recorded by LASA at distances from 18° to 98°. We use a modified version of the Generic Array Processing software package to identify ICS waves on the basis of travel time, back azimuth, ray parameter, amplitude, and coherence. There are 44 events that produce clear ICS waves. We then perform forward modeling of the observed ICS waves using a Monte Carlo seismic phonon method that allows for multiple scattering along the raypath. Most of the ICS waves appear without a visible *PKiKP* phase, initially grow in time, and have a spindle-shaped envelope. The duration, risetime, and decay rates of the observed ICS waves can be best explained by small-scale volumetric heterogeneities in the outermost few hundred kilometers of the inner core. The average *Qc* value for the 44 events is ~600. Most clear ICS waves are found for raypaths sampling the Pacific Ocean and Asia, and relatively few observations are from the Atlantic Ocean, roughly consistent with the recently observed hemispheric difference in the inner-core structure.

Citation: Peng, Z., K. D. Koper, J. E. Vidale, F. Leyton, and P. Shearer (2008), Inner-core fine-scale structure from scattered waves recorded by LASA, *J. Geophys. Res.*, *113*, B09312, doi:10.1029/2007JB005412.

1. Introduction

[2] The Earth's inner core is one of the most dynamic parts of the Earth's interior. Although the inner core is mainly composed of iron and other light elements, its detailed structure is far from well known. Recent studies have found strong lateral heterogeneities inside the inner core with a wide range of length scales [*Tromp*, 2001; *Song*, 2003, and references therein]. Observations of backscattered *PKiKP* coda waves provide evidence that the outermost few hundred kilometers of the inner core contains heterogeneity on the length scale of a few kilometers [*Vidale and Earle*, 2000]. These waves, termed inner-core scattering (ICS) waves, travel along a similar path to the inner-core–reflected waves *PKiKP* (Figure 1a), follow immediately after the expected *PKiKP* arrival, grow to a peak at ~50 s, and slowly decay over time. *Koper et al.* [2004] found additional evidence of the ICS waves from a global study using seismic data recorded by array stations of the International Monitoring System.

[3] Although it has been suggested that the ICS waves could be produced by reverberations at the inner-core boundary (ICB) [*Poupinet and Kennett*, 2004], synthetic calculations using a single-scattering approximation and ray theory favor the idea that the spindle shape, or initial growing *PKiKP* coda, can only be produced from volumetric heterogeneities located inside the shallow portion of the inner core [*Leyton and Koper*, 2007a]. Since the ICS waves are backscattered in the top few hundred kilometers of the inner core, they provide one of the highest-resolution tools for better understanding of the fine-scale structure of the inner core. This has important implications for our knowledge of core processes, including the solidifying of the inner core from the liquid outer core, and the generation of the Earth's magnetic field. Temporal changes in ICS waves can be used to further refine the differential rotation rate of the Earth's inner core [*Vidale et al.*, 2000].

[4] The ICS waves reported by *Vidale and Earle* [2000] were originally observed in seismic data produced by 12 earthquakes and four nuclear explosions in the distance range of 58° to 73°, and recorded by the Large Aperture Seismic Array (LASA) between 1969 and 1975. Here we use the same data set, and find a total of 44 events generating high-quality ICS waves in the distance range

[1]School of Earth and Atmospheric Sciences, Georgia Institute of Technology, Atlanta, Georgia, USA.
[2]Department of Earth and Atmospheric Sciences, Saint Louis University, St. Louis, Missouri, USA.
[3]Department of Earth and Space Sciences, University of Washington, Seattle, Washington, USA.
[4]Departamento de Geofísica, Universidad de Chile, Santiago, Chile.
[5]Institute of Geophysics and Planetary Physics, Scripps Institution of Oceanography, University of California, San Diego, La Jolla, California, USA.

0148-0227/08/2007JB005412$09.00

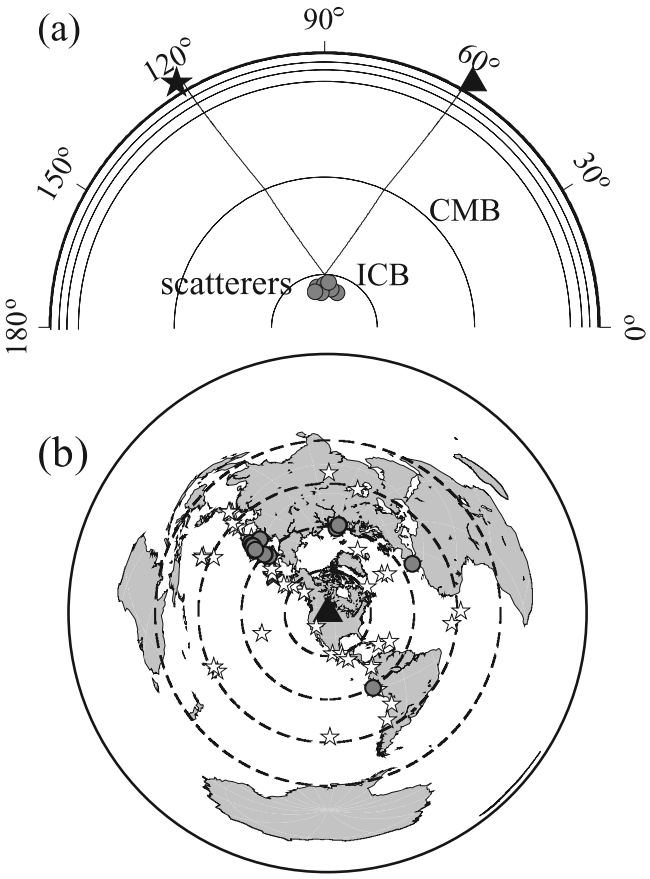

Figure 1. (a) Raypath for *PKiKP* at a distance of 60°. At this range, most of the energy is transmitted across the inner-core boundary. The inner-core scattering (ICS) wave path is very similar to that of the *PKiKP*. (b) A map showing the epicentral locations of 78 events (stars) and the distances to the center of the LASA array (black triangle) by an azimuthal equidistant projection. The black circles mark the 16 events that were used in the study of *Vidale and Earle* [2000]. The dashed circles mark the distance at 30° increments.

of 34° to 98°. Most of the ICS waves have a spindle-shaped envelope, and the durations shrink with increasing distances. We also perform forward modeling of the observed ICS waves using a Monte Carlo seismic phonon method that allows for multiple scattering events between source and receiver [*Shearer and Earle*, 2004]. In addition, we find that most ICS waves are coming from raypaths sampling the Pacific Ocean and Asia, and relatively few observations from the Atlantic Ocean. This is roughly consistent with the recently observed hemispheric pattern of the inner-core structure [*Creager*, 1999; *Niu and Wen*, 2001; *Wen and Niu*, 2002; *Cao and Romanowicz*, 2004; *Koper et al.*, 2004; *Leyton and Koper*, 2007b; *Cormier*, 2007].

2. LASA Array and Data Selection

[5] We use the short-period array data generated by 152 events (Figure 1b) and recorded by LASA, which was in operation from 1968 to 1978 [*Frosch and Green*, 1966; *Hedlin et al.*, 2000]. It consisted of up to 525 short-period (~1 Hz) borehole sensors with an aperture of ~200 km. The E and F outer rings were turned off before 1974. Because there were large travel time anomalies associated with the outer rings [*Engdahl and Felix*, 1971], we only use data recorded by the inner four rings (A, B, C, and D) in this study, representing 13 subarrays and at most 207 stations (Figure 2). The corresponding station coordinates are listed in Table S1.[1]

[6] We select events in the distance range of 12–98°, where *PKiKP* is precritical and most energy incident on the ICB is transmitted rather than reflected. We visually inspect all the waveforms, and remove those events with no data or strong glitches in the time window of 890–1340 s, which roughly corresponds to 100 s before the minimum, and 250 s after the maximum theoretical arrival time of *PKiKP* on the basis of Preliminary Reference Earth Model (PREM) [*Dziewonski and Anderson*, 1981]. After the selection process, we obtain a total of 78 events for further analysis. The event information, epicentral distance, back azimuth, and quality of the *PKiKP* and ICS waves (as described in section 4) are listed in Table S2.

3. Analysis Procedure

[7] We use a modified version of the Generic Array Processing (GAP) Software Package [*Koper*, 2005] (The GAP source code are available at ftp://ftp.eas.slu.edu/pub/koper/gap.1.0.tar.gz) to analyze the data. We first filter the records with a three-pole Butterworth band-pass filter with corners at 0.67 and 1.33 Hz. Next, we apply a sliding window slowness analysis for all data generated by the 78 events. We use a time window of 2 s with a 50% (1 s) overlap. For each time segment, we perform a search over a grid of potential 2D slowness vectors, and select as optimal the slowness vector that gives the highest beam power. Beam power is defined as the root-mean-square (rms) amplitude over the selected time window, with amplitude proportional to the ground velocity. The waveform coherence is also computed by stacking the instantaneous phases of the shifted traces [e.g., *Schimmel and Paulssen*, 1997].

[8] An example of the GAP output is given in Figure 3. This event was the first of the two closely located nuclear explosions at Novaya Zemlya that were used in *Vidale et al.* [2000] to constrain the inner-core differential rotation. The direct *P* wave is slightly clipped. Two mantle phases, *PcP* and *PP,* are nearly buried in the *P* coda waves. The direct *PKiKP* wave is not prominent at a distance range of ~60°. However, there is a clear signal that persists for ~200 s after the expected *PKiKP* arrival, which is marked by a drop to near-zero slowness and a slight increase in beam power and coherence. This signal, termed ICS waves by *Vidale and Earle* [2000], is most likely scattered in the upper few hundred kilometers of the inner core and follows a similar raypath to that of the core-reflected phase *PKiKP* (Figure 1). *PKKP*, which reflects from the underside of the core-mantle boundary, does not appear at 60° as a distinct arrival but as a broad envelope of scattered energy (termed $PKKP_X$ by *Earle and Shearer* [1998]) around the theoretical $PKKP_{DF}$ time. Finally, $P'660P'$, $P'440P'$, and $P'P'$, the underside

[1] Auxiliary materials are available in the HTML. doi:10.1029/2007JB005412.

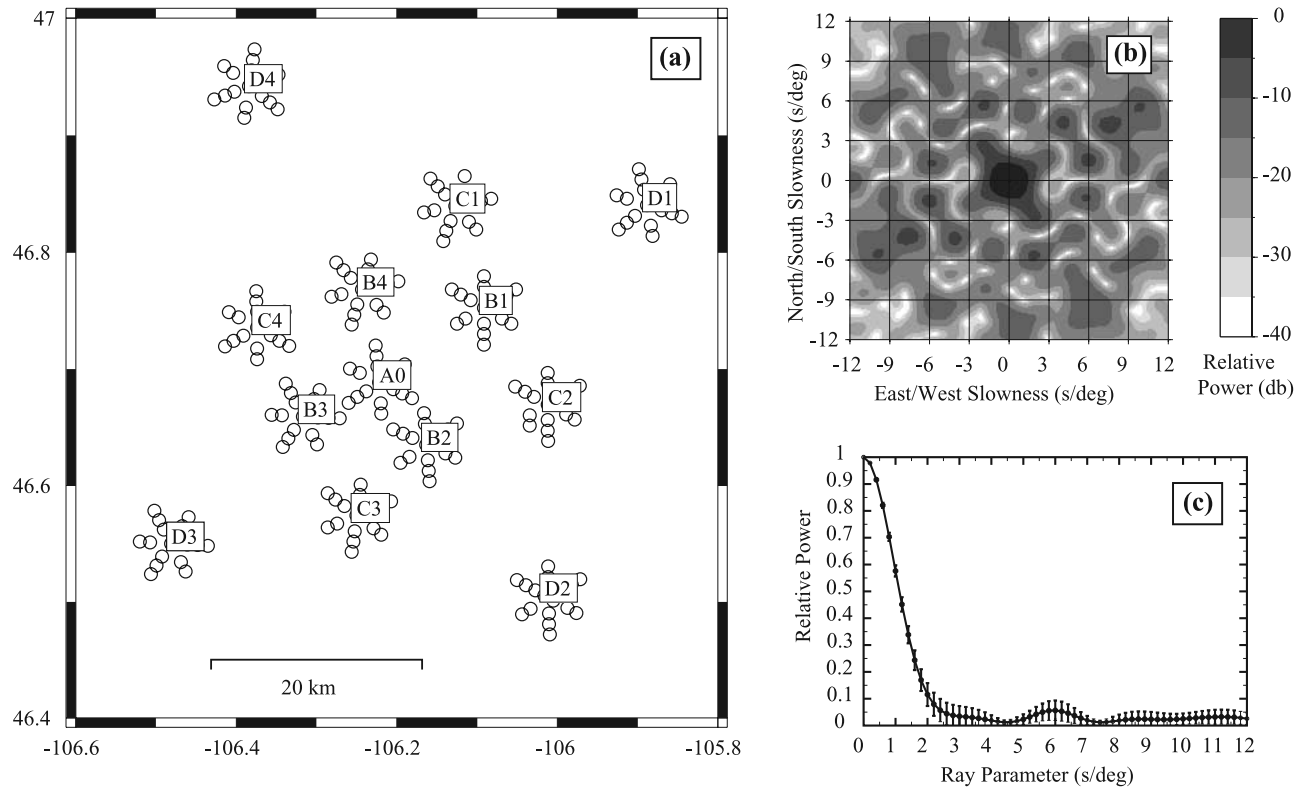

Figure 2. (a) Geometry of the inner four rings of LASA subarrays that are used in this study. (b) The corresponding array response function (ARF) for a frequency of 1 Hz. (c) The azimuthally averaged ARF.

reflections from the 660 km and 440 km mantle discontinuities and the Earth's free surface, respectively, appear at 2200–2400 s.

[9] We note that there is an abrupt change in back azimuth and slowness for the ICS waves occurs about 100 s after the *PKiKP* arrival, and the back azimuth is scattered rather than following the minor arc direction. This is likely due to the decaying *P* coda and gradually increasing ICS amplitude (Figure 3i). Only after about 100 s does the grid search program pick the back azimuth and slowness corresponding to the ICS as the best fitting parameters. In addition, the ICS waves cover a range of slowness around the expected *PKiKP* arrival, which is very near zero slowness. Some of them may be associated with negative slowness, and hence result in back azimuths similar to major arc phases such as *PKKP* and $P'P'$.

[10] Next, we construct envelope beams with linear summation on the basis of the theoretical *PKiKP* slowness from PREM [*Dziewonski and Anderson*, 1981]. We then stack 21 envelopes with ±1 s/deg around the expected *PKiKP* slowness, and smooth the resulting envelope stack by a median operator with a half width of 20 data points (2 s). The 2 s/deg slowness window captures most of the ICS wave energy around the *PKiKP* slowness (Figure 3). We also compute a noise envelope by averaging 21 envelopes between −9 and −7 s/deg, where no clear phase is expected or observed around the *PKiKP* arrival [*Vidale and Earle*, 2000]. The choice of the slowness window for noise is somewhat arbitrary, but helps to define a background noise level that is relatively stable across a wide range of slowness. The noise is removed by squaring the signal envelope, subtracting the square of the line fit to the noise, and taking the square root [*Vidale and Earle*, 2000]. An example of this procedure is shown in Figure 4 for the same nuclear event. The resulting ICS envelope has a clear spindle shape, building to a peak at about 50 s and then slowly decaying afterward.

4. Variations of *PKiKP* and ICS Waves With Magnitude and Locations

[11] We assign a quality index for *PKiKP* and ICS generation to all 78 events on the basis of visual inspection of the slowness analysis output (Figure 3) and the resulting ICS envelope (Figure 4). Before assigning the qualities, we check the signal-to-noise ratio (SNR) of the resulting envelope, and require that the average amplitude within 25 s of the expected *PKiKP* arrival be at least 1.5 times larger than the preevent noise level (30 to 5 s before the expected *P* arrival). Eleven envelopes do not satisfy this criterion. Next, we assign one of the following three quality indices to the *PKiKP* and ICS waves for each event: (2) conclusive, (1) inconclusive, and (0) negative. We require that the events with a quality of 2; for *PKiKP* have a sharp arrival at the expected arrival and slowness, and that those events with a quality of 2 for ICS waves have persistent coda energy with the expected *PKiKP* slowness clearly above the preevent noise level. For example, the nuclear event presented in Figures 3 and 4 has a quality of 0 in *PKiKP*, and 2 in ICS waves. Additional examples corresponding to other qualities are shown in Figure 5.

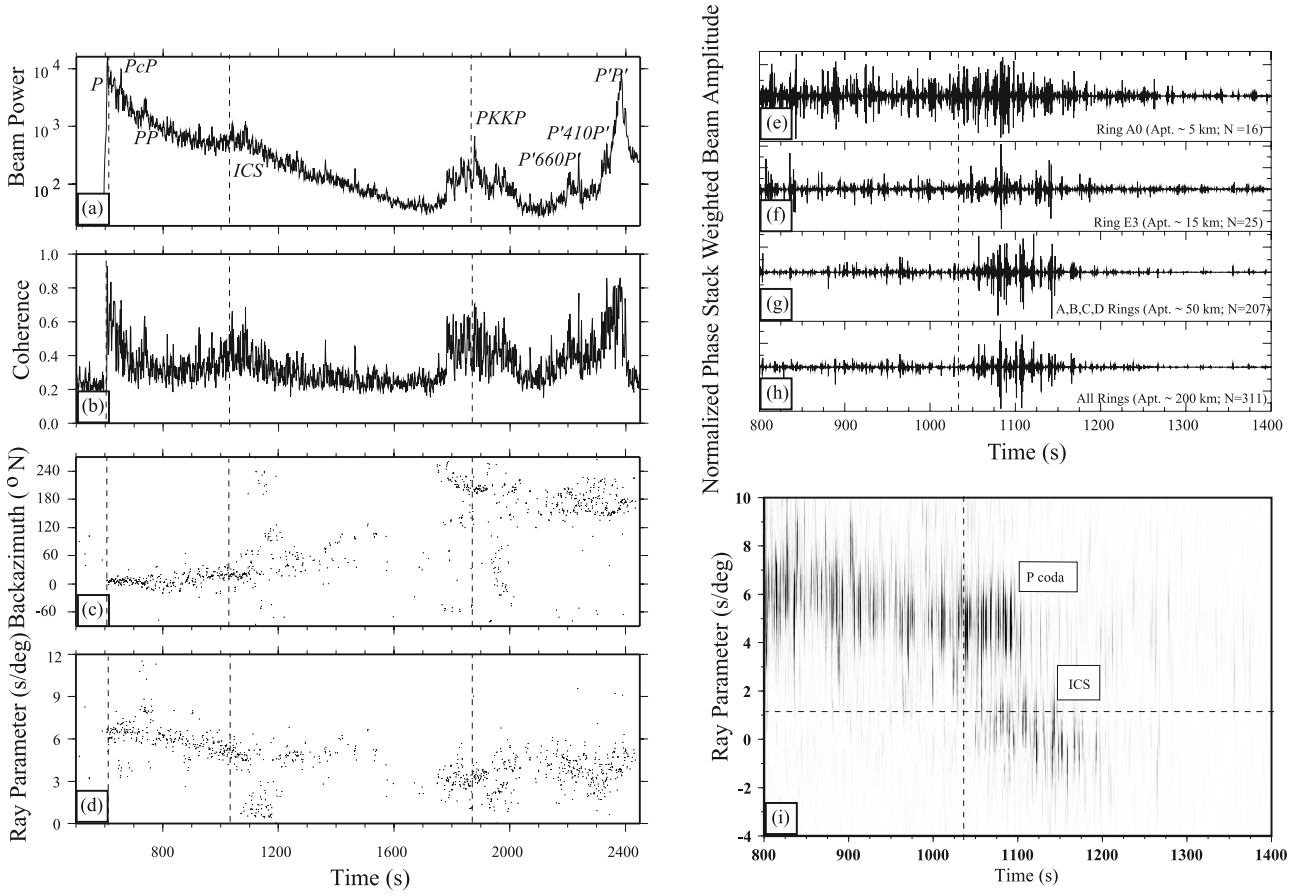

Figure 3. Example output of the Generic Array Processing software package for an m_b = 6.5 nuclear explosion in 1971 (evid 710927_0559) at Novaya Zemlya. (a–d) The best fitting beam power, coherence, back azimuth, and slowness in the 1-Hz frequency band, with a window length of 2 s and a window spacing of 1 s. The vertical dashed lines mark the arrival times of the *P*, *PKiKP*, and $PKKP_{DF}$ predicted by the Preliminary Reference Earth Model. Figures 3c and 3d only show data points with coherence of at least 0.3. (e–h) Phase weight beam formed at the theoretical *PKiKP* slowness using data recorded by different rings. (i) Slowness versus time plot of the seismic energies recorded by LASA around the theoretical *PKiKP* arrival (vertical dashed line). The *P* coda and ICS energies are marked. The horizontal dashed line marked the expected slowness of the *PKiKP* arrival.

The qualities of the *PKiKP* and ICS waves for all 78 events are listed in Table S2.

[12] The quality of *PKiKP* and ICS waves is plotted against the event magnitude and distance in Figure 6. A total of 44 events, roughly 56%, have a quality index of 2 (conclusive) for ICS observation. In comparison, only 14 events (18%) receive a quality index of 2 for *PKiKP* observation. There is a weak correlation between the quality and the event magnitude. Eight out of 11 events with magnitudes less than 5.5 have low SNR that prevents us from assigning quality to them. The quality of both ICS and *PKiKP* waves correlates with distance. Thirty out of 40 events (75%) in the distance range of 55–90° generate ICS waves with quality 2. In comparison, only two events (5%) in this distance range produce *PKiKP* waves with quality 2. Most of the high-quality *PKiKP* phases are observed at short- and large-distance ranges. This is likely because the reflection coefficient of the direct *PKiKP* phases drops to a low value in the intermediate distant range. Thus, nearly all of the energy is transmitted through the inner-core boundary. The anticorrelation between the quality of ICS and *PKiKP* waves suggests that the coda of the *PKiKP* waves are mostly generated by backscattering in the uppermost layers of the inner core with strong heterogeneities, instead of scattering from irregularities on the ICB, the core mantle boundary (CMB), or volumetric scattering in the lower mantle [*Leyton and Koper*, 2007a, 2007b].

[13] We find that most of the ICS waves with conclusive quality come from the raypaths sampling the Pacific Ocean and polar paths (Figure 7). Only two of nine events in the Atlantic Ocean produce conclusive ICS waves. Although the number of events in the Atlantic Ocean is relatively small, and we cannot totally rule out the influences of focal mechanisms and SNR, our observation is roughly consistent with the hemispheric patterns of the inner-core structure inferred from anisotropy, the velocity jump at the inner-core boundary, attenuation [e.g., *Creager*, 1999; *Niu and Wen*,

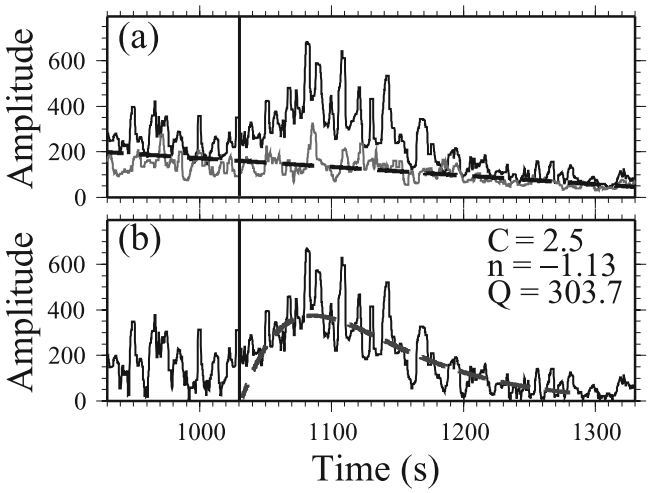

Figure 4. (a) A zoom-in plot of the stacks for the ICS waves (black line) across the slowness range of 0.2 to 2.2 s/deg around the expected *PKiKP* slowness and for the background noise (gray line) around −9 to −7 s/deg where discrete arrivals are not expected around the *PKiKP* arrival (vertical line). The dashed line is a straight line fit to the noise. (b) The ICS signal after removing the noise fit in Figure 4a. The dashed line is a best fitting coda envelope with three parameters marked in Figure 4b (right).

2001; *Wen and Niu*, 2002; *Cao and Romanowicz*, 2004; *Cormier*, 2007], and scattering [*Koper et al.*, 2004; *Leyton and Koper*, 2007b].

5. Decay Rate of the ICS Envelope

[14] We quantify the decay rate of the ICS envelope with the quality factor *Qc* [*Leyton and Koper*, 2007b], as has been done in studying crustal heterogeneities [e.g., *Mitchell*, 1995]. On the basis of a single-scattering assumption [*Sato and Fehler*, 1998], the energy, or velocity squared of ICS waves, is given by

$$v^2(t) = A\frac{1}{t^{2n}}\exp(-2\pi Qc^{-1}ft),$$
$$\ln(v(t)) = C - n\ln(t) - \pi Qc^{-1}ft, \quad (1)$$

where $C = 1/2\ln(A)$ is proportional to source excitation, path and site effects, and n and Qc represent geometric spreading and quality factors, respectively. We fit the data starting 10 s after the predicted *PKiKP* arrival to avoid contamination of the direct phase. The *Qc* value is mostly constrained by the tail of the coda and is sensitive to the material properties of the inner core. We also allow the geometric spreading factor, n, to vary. Positive and negative values of n correspond to normally decaying and initially growing codas, respectively [*Frankel and Clayton*, 1986; *Leyton and Koper*, 2007b]. An example of the *Qc* fitting is shown in Figure 4 for initially growing codas.

[15] The measured *Qc* values versus epicentral distances are shown in Figure 8. Only three events with epicentral distances larger than 85° have normal decaying coda with $n > 0$. The remaining 41 events have growing *PKiKP* coda with $n < 0$. *Leyton and Koper* [2007a] performed synthetic calculations of ICS waves from several distinct places inside the Earth, and concluded that the initial growing ICS waves can only be generated by volumetric scattering in the inner core. Our observations of initial growing ICS waves with $n < 0$ in a wide distance range are consistent with their synthetic modeling. The normal decaying coda at larger distances is likely caused by a combined effect of increasing *PKiKP* amplitude, and overlapping of coda from previous phases such as *PcP*. The geometric average of the *Qc* values is 566, although individual values have large scatter. This value is similar to the average *Qc* value of ∼500 observed from a global data set of ICS waves [*Leyton and Koper*, 2007b].

6. Synthetic Modeling of the ICS Envelopes

6.1. Comparison of Phonon Simulations for Different Models

[16] The *Qc* value measured in the previous section is based on the single-scattering assumption. In this section we

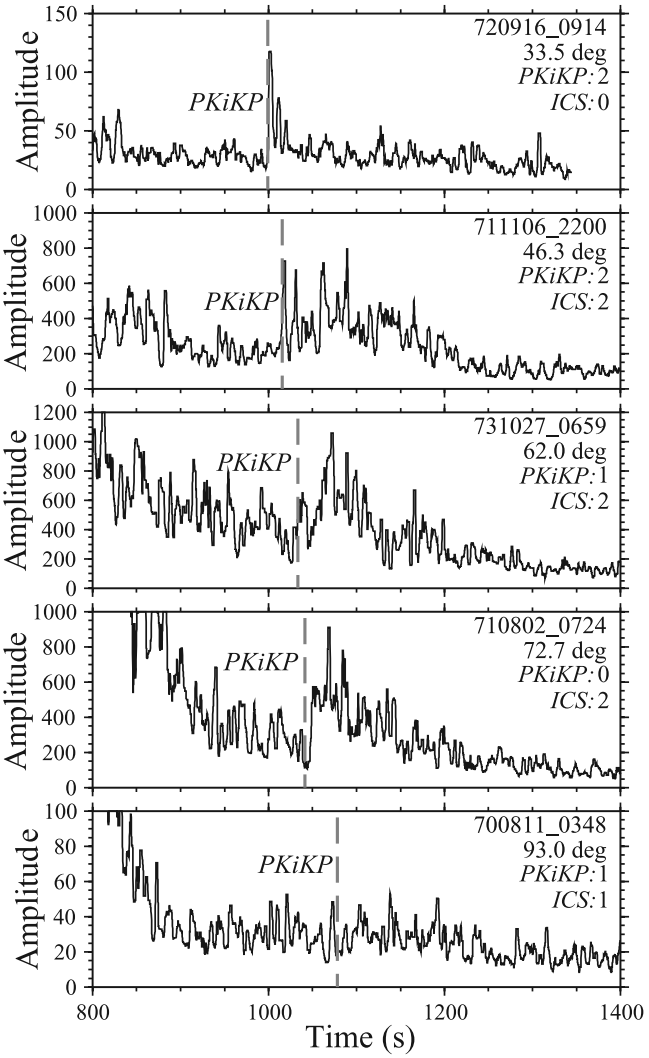

Figure 5. Examples of noise-removed envelopes at different distance ranges with (right) different qualities of the *PKiKP* and ICS generation. The vertical dashed line marks the expected *PKiKP* arrival.

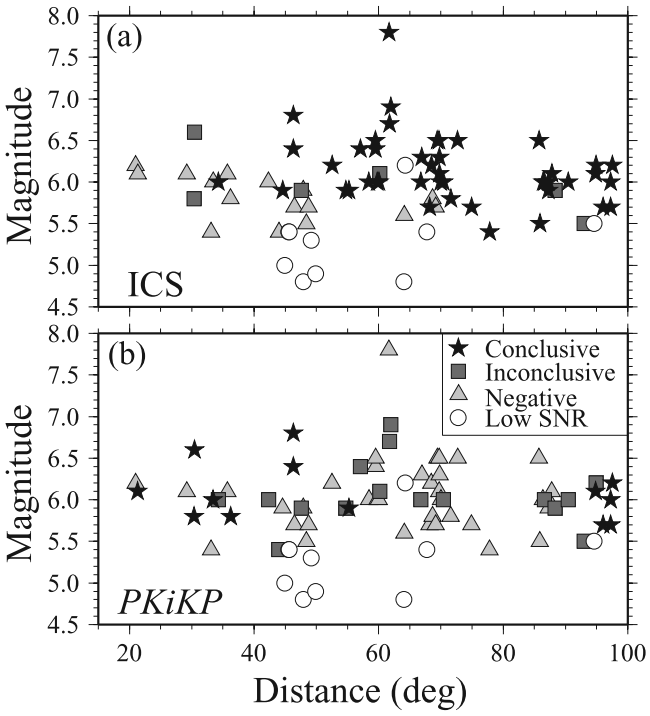

Figure 6. Magnitude and distance distribution of the 78 events. The data ranked as conclusive, inconclusive, or negative for (a) ICS waves and (b) *PKiKP* are shown as stars, squares, and triangles, respectively. The white circles mark the events with low signal-to-noise ratio (SNR).

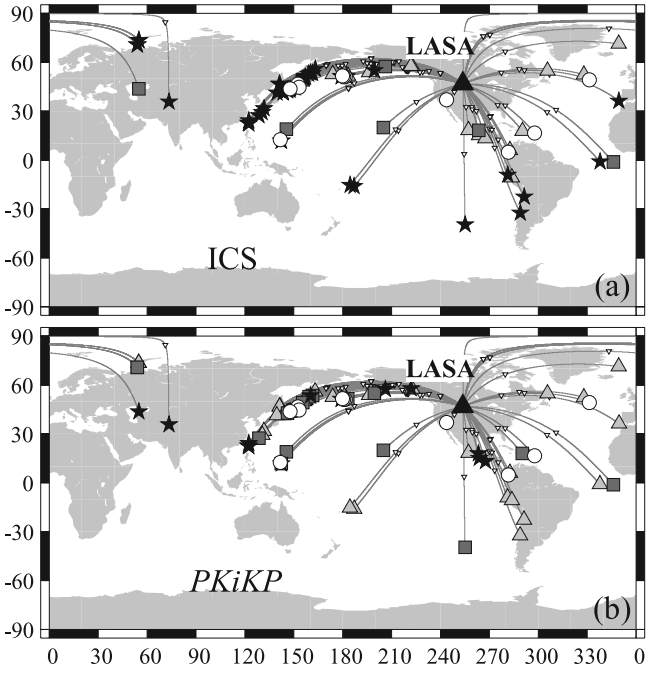

Figure 7. Surface projections of the *PKiKP* raypath for the 78 events. The data are ranked as conclusive (star), inconclusive (square), and negative (triangle) for (a) ICS and (b) *PKiKP*, respectively. The white circles mark the events with low SNR. The small inverted triangles denote the bounce point at the inner-core boundary.

model the ICS envelopes using a Monte Carlo seismic phonon method that allows for multiple scattering between source and receiver [*Shearer and Earle*, 2004]. This approach generates synthetic codas for radial Earth models in which heterogeneity is parameterized by an exponential autocorrelation function that depends on three parameters: an RMS velocity perturbation ε, an RMS density perturbation υ, and a correlation length a. These parameters can vary from layer to layer within the Earth, and so nonuniform models are easily evaluated. The *P*- and *S*-velocity perturbations are assumed to be equal. However, the scattering coefficients are explicit functions of the Poisson's ratio in a given layer. Therefore, scattering in the inner core, which has an unusually large Poisson's ratio, is properly accounted for. Travel times and amplitudes are computed using classical ray theory, and anelastic effects are also included.

[17] A comparison of phonon simulations for two Earth models is shown in Figure 9a. Although the method generates the complete wavefield across all space and time, "codagrams" at specific distances can be easily extracted. Each codagram in Figure 9 shows the vertical component amplitude as a function of time at a distance of 60° for a source depth of 0 km. We radiate only *P* energy from the source and use an isotropic pattern appropriate for explosions. The model contains 2% RMS velocity perturbations at 4 km scale length for the upper 600 km of the mantle, and 0.5% RMS velocity perturbations at 8 km scale length for the remainder of the mantle. Density perturbations are calculated as 0.8 of the velocity perturbations. The intrinsic attenuation $Q\alpha$ model is 227 for 0 to 220 km, 1383 for 220 km to the CMB, and 360 for the inner core. This model is very similar to the mantle scattering and intrinsic attenuation model of *Shearer and Earle* [2004] derived from modeling teleseismic *P* coda, except that our new model has weaker velocity perturbations (and less scattering) in the uppermost 200 km. We found that this change was necessary in order to produce suitably impulsive *PcP* and *PKP* arrivals.

[18] One of the models illustrated in Figure 9a also possesses scattering in the upper 300 km of the inner core

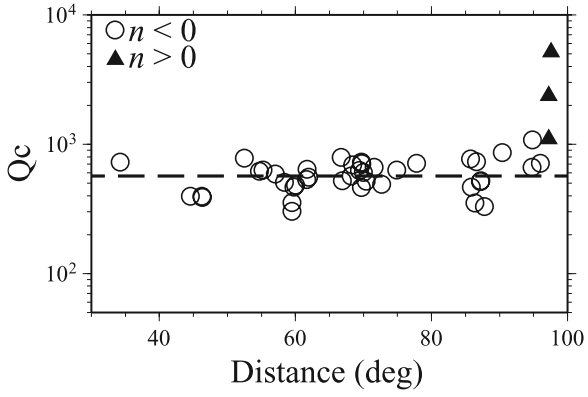

Figure 8. Measured *Qc* values as a function of epicentral distances. The circles and triangles mark events with initial growing ($n < 0$) and normal decaying ($n > 0$) codas, respectively. The horizontal dashed line marks the geometric average of the *Qc* values.

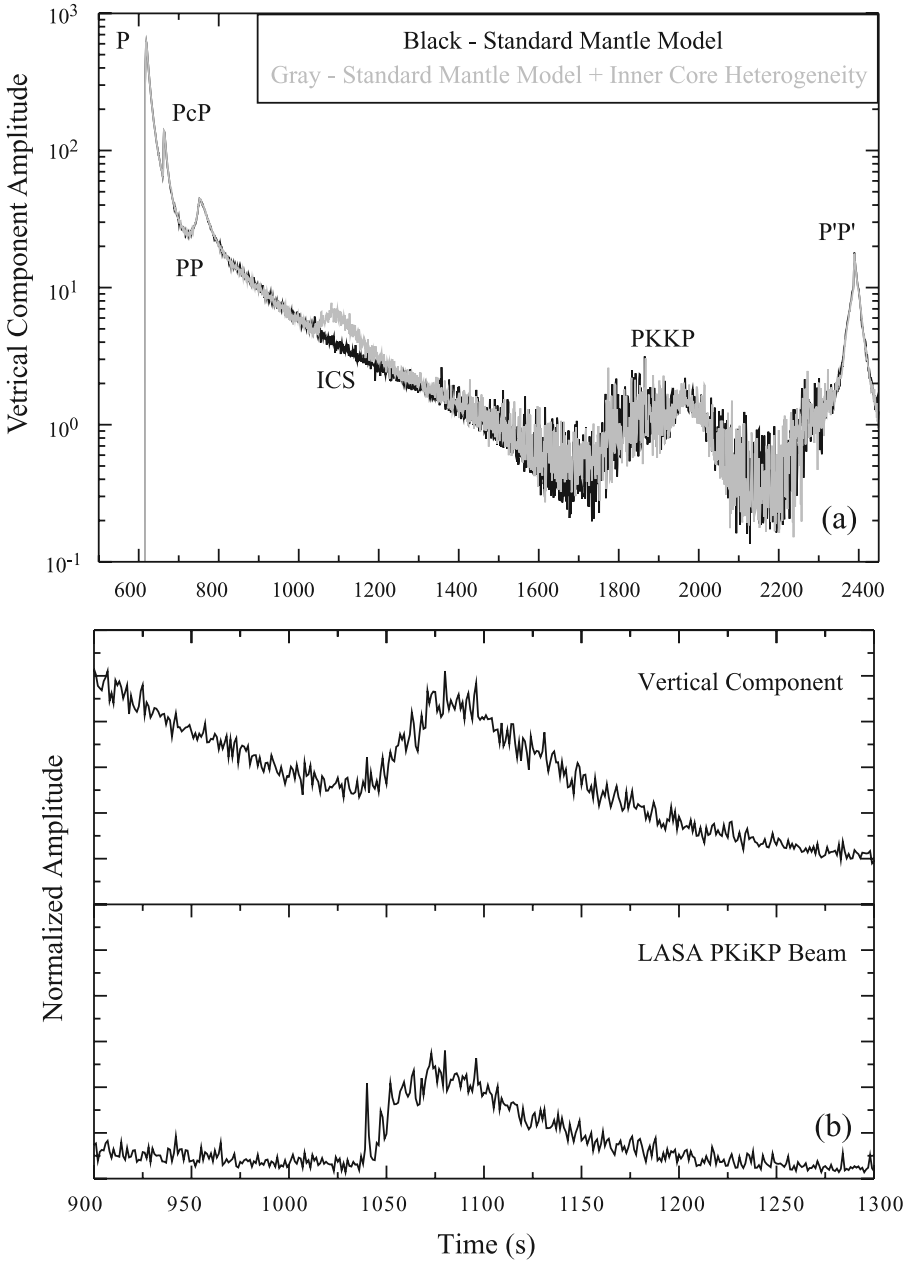

Figure 9. (a) Synthetic codagrams generated at a distance of 60° for an event located at the surface. Time is relative to the origin time, and amplitude is in arbitrary units proportional to the envelope of ground velocity on a vertical component seismometer. Both models possess scattering throughout the mantle, however only the model indicated by the gray curve possesses scatterers in the inner core. (b) Synthetic codagrams at 60° for an Earth model with scattering in the inner core. The expected *PKiKP* arrival time is about 1040 s. Figure 9b (top) shows the output in which all energy, no matter the incoming ray parameter, contributes to the amplitude at a given time. Figure 9b (bottom) shows the effect of applying the azimuthally averaged LASA ARF. This has the effect of attenuating energy arriving at directions significantly different than the direct *PKiKP* wave and produces a codagram that can be directly compared to the observed envelope of a LASA beam formed with the theoretical *PKiKP* slowness vector.

with an RMS velocity perturbation ε of 1.2%, no density perturbations, and a scale length a of 2 km, as determined in *Vidale and Earle* [2000]. Both codagrams match the general character of the observed data with clear peaks at the arrival times of dominant phases such as *P*, *PcP*, *PP*, *PKKP*, and *P'P'*, but only the model with ICS is able to generate a significant growing coda following the arrival of *PKiKP*. We experimented with other mantle models that included especially strong scattering in the lowermost mantle, as have been suggested by previous studies. The results are essentially the same as shown in Figure 9a. Only models with ICS are able to produce emergent, growing *PKiKP*

codas at ranges of approximately 50–75° observed by *Vidale and Earle* [2000] and in this study. This is consistent with the simulated ICS waves codas for various models of deep Earth heterogeneity using classical single-scattering techniques [*Leyton and Koper*, 2007a].

6.2. Forward Modeling of the ICS Envelope With the Phonon Method

[19] In order to compare the phonon simulations directly to the data, the array response function (ARF) of LASA must be considered. The full ARF at 1 Hz for the A, B, C, and D rings of LASA is shown in Figure 2. It is has a high degree of radial symmetry and little is lost by neglecting azimuthal variations. For each distance bin in which pre-critical *PKiKP* exists, we reduce the power of the incoming phonon on the basis of its deviation from the theoretical *PKiKP* ray parameter. As shown in Figure 2, a deviation of more than about 3 s/deg in 2D slowness space results in very little contribution to the codagram, and even for a 1 s/deg deviation only about half the energy contributes. The sharpness of this wave number filter is due to the relatively large aperture of LASA. The results of this procedure are a series of synthetic *PKiKP* codagram beams that can be compared directly to the observed data. An example is shown in Figure 9b. A related approach is to form beams at a series of equally spaced ray parameters creating a synthetic slantstack that can be compared to observations.

[20] To model the ICS observations we use only the explosion data recorded at LASA, which consists of four events near 60° and two events near 45°. The reason for this is that the explosions have isotropic radiation patterns and so the observed *PKiKP* coda can be normalized by the observed *PcP* amplitude without considering the effects of source take off angles. Although the phonon method assumes isotropic radiation pattern, it has been applied to model coda generated by natural earthquakes with variable focal mechanisms [*Shearer and Earle*, 2004, 2008]. This could be justified by smearing of radiation patterns during high-frequency wave propagation, and averaging over many earthquakes and stations with different take off angles [*Shearer and Earle*, 2008]. However, we took a conservative approach in the current work by only modeling the 6 explosions.

[21] For each event, we form a standard linear beam using the theoretical *PKiKP* slowness vector and the A, B, C, and D rings of LASA. The *PKiKP* phase itself is unsuitable to be the reference phase because it is often too small to be observed in the data. So we form an equivalent *PcP* beam and use the peak *PcP* amplitude to normalize the *PKiKP* beam [e.g., *Vidale and Earle*, 2000]. As expected, we find the *PKiKP* coda amplitude to be about 1–3% of the *PcP* amplitude. We next generate the envelope of the *PKiKP* beam, fit a line using data from 100 s before *PKiKP* and 200–300 s after *PKiKP*, and remove the trend. This compensates for the low-slowness component of signal-generated noise that occurs during the *PKiKP* coda window but is unrelated to the inner core. The detrended data are then smoothed with a 2 s, sliding window, median filter. Finally, the six beams are aligned on the *PKiKP* arrival time and stacked.

[22] For a given Earth model we generate synthetic *PKiKP* codagrams at 45° and 60° and perform the same processing used on the data. Removal of the residue coda is necessary because the phonon method generates its own slowly decaying, low-slowness energy during the *PKiKP* time window from scattering in the crust and mantle (Figure 9b). We then create a stack aligned on the *PKiKP* time with the 60° synthetic weighted twice as much as the 45° synthetic, in accordance with the data stack. The final model stack is compared with the data stack using an RMS metric for 200 s after the *PKiKP* arrival time.

[23] Figure 10a shows the fit of the two previously published models of inner-core heterogeneity. The model suggested by *Vidale and Earle* [2000] (rms velocity perturbation ε = 1.2%, correlation length a = 2 km) fits the data reasonably well, although the amplitude is slightly larger than the data. This may be because the multiple scattering approach used here generates larger coda energy for a given model than the single-scattering approach used in *Vidale and Earle* [2000]. In addition, the specific data set used here and the processing of the data are slightly different as compared with the previous study. The model proposed by *Cormier and Li* [2002] (rms velocity perturbation ε = 8.4%, correlation length a = 9.8 km) predicts *PKiKP* coda waves that are even larger. However, that model was determined from forward scattered energy (*PKIKP* waves) assuming no component of anelastic attenuation and so is properly interpreted as an upper bound on the scattering strength of the inner core.

[24] Evaluation of candidate Earth models is computationally intensive because only a relatively small number of phonons contribute to the *PKiKP* coda, and the smoothness of simulated codas scales as the square root of the number of phonons. We find that about a billion phonons are required to generate robust *PKiKP* codas, corresponding to several hours of real time on the 16 node, dual 2 Ghz processor, Beowulf cluster maintained by the Department of Earth and Atmospheric Sciences at the Saint Louis University. Because of this, it is not feasible to do a complete grid search of the relevant portion of the model space. Instead, we use a trial-and-error approach to find high-quality models and build intuition about the trade-offs between the two formal model parameters: RMS velocity perturbation in the outer 300 km of the inner core (ε) and the corresponding scale length of the heterogeneities (a). The two model parameters are anticorrelated in the sense that either larger ε or smaller a leads to larger *PKiKP* coda waves. Hence, high-quality models can be found for a range of a values by making the proper adjustment to ε (Figure 10b).

[25] All the parameter combinations reported above were determined using a Qp of 360 for the inner core, and they change somewhat if different values of Qp are assumed. Higher Qp values require weaker models of inner-core scattering to provide equivalent fits to the ICS waves. We experimented with various Qp values and found that the major effect is a uniform scaling of the coda envelope with relatively little change in the shape or the decay rate. Furthermore, reasonable changes to Qp generate relatively small changes in the envelopes. For example, changing Qp from 300 to 600 results in the peak ICS amplitude changing from 1.0% to 1.4% of the *PcP* amplitude with ε = 1.0% and a = 4.0 km (Figure 10c).

[26] The assumed thickness of the scattering layer in the inner core also has an effect on synthetic ICS envelopes. For all of the results presented above we used a thickness of 300 km, in accordance with previous studies [*Vidale and*

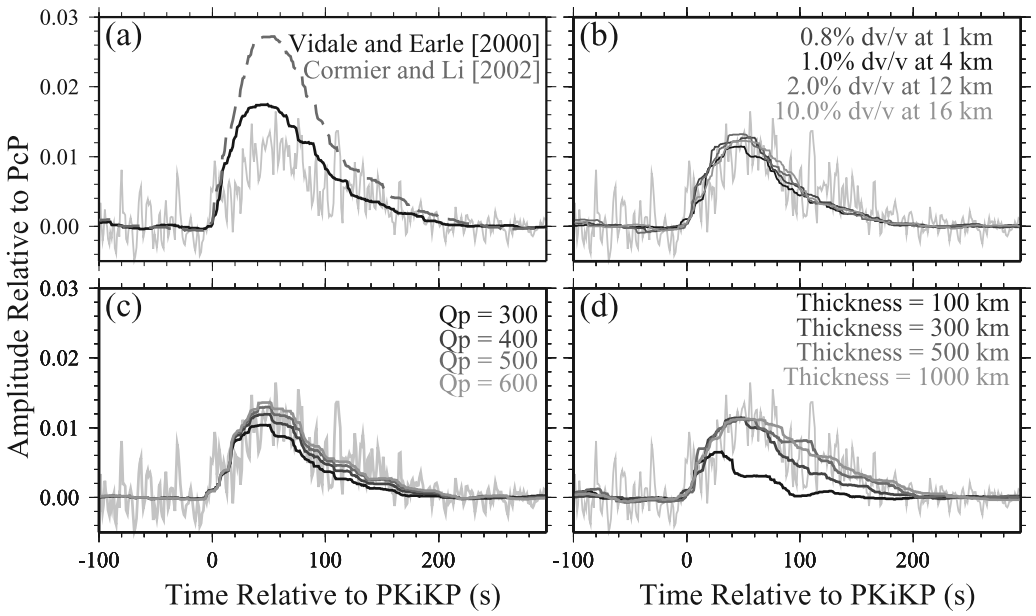

Figure 10. (a) Phonon simulations based on the two published models of inner-core heterogeneity [*Vidale and Earle*, 2000; *Cormier and Li*, 2002] relative to the stacked LASA data from six nuclear explosions (light gray line). The *Cormier and Li* [2002] model was designed to account for both intrinsic and scattering attenuation and so should be considered an upper bound. (b) Four of the high-quality models of inner-core heterogeneity found in this study. No density perturbations are included. Considering uncertainties in the processing, the four models have equivalent levels of fit to the data. Note the trade-off between RMS velocity variation and correlation length. (c) Comparison of the stacks of six nuclear explosions (light gray line) with synthetic codagrams using different *Qp* values. (d) Comparison of the stacks of six nuclear explosions (light gray line) with synthetic codagrams using different thickness of the ICS layer.

Earle, 2000; *Koper et al.*, 2004; *Leyton and Koper*, 2007b]. Using significantly thicker layers leads to a decrease in the decay rate of the *PKiKP* coda envelope (and a marginally better fit to the observations) but almost no change to its peak value (Figure 10d). Because of all the trade-offs, it is not possible to estimate robustly the maximum depth of the scattering layer, and we cannot rule out the possibility that the entire inner core possesses fine-scale heterogeneity. Like previous studies we find that relatively thin scattering layers (50–100 km) are generally not able to reproduce the broadly emergent, slowly decaying ICS observed in data (Figure 10d). Instead, models with thin scattering layers preferentially concentrate ICS near the beginning of the coda. It's possible that with a different scattering theory a thin layer may lead to a more broadened coda, however in all of our experiments a relatively thick layer was required. In order to determine more precise estimates of the scattering properties of the inner core, it will be necessary to model jointly backscattered energy in the form of the ICS waves with forward scattered energy in the form of *PKIKP* amplitudes and possibly *PKIKP* coda waves [e.g., *Cormier*, 2007]. Additionally, it will be necessary to explore the effect of nonisotropic distributions of heterogeneities [i.e., *Hong and Wu*, 2005] in which scatterers have preferred orientations or aspect ratios.

7. Growth of Envelope With Distance

[27] Figure 11 shows the noise-removed envelope stacks by every 5° around the *PKiKP* arrivals for events that have

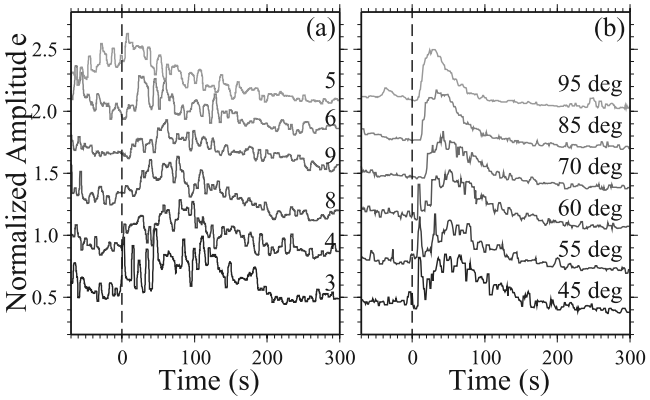

Figure 11. (a) Noise-removed envelope stacks by every 5° around the *PKiKP* arrivals for events that have conclusive quality for the ICS observation. All envelopes are aligned at the expected *PKiKP* arrival time. The number in Figure 11a (right) shows the total number of events in each stack. We only show stacks that have at least three or more waveforms within each 5°. (b) Synthetic codagrams at different distances using the following parameters: RMS velocity perturbation of 1.0% and a corresponding scale length of the heterogeneities of 4 km. The number in Figure 11b (right) shows the distance range in degrees.

conclusive quality of the ICS observation. We find that envelopes within 45–75° have the most clearly growing *PKiKP* coda. Similar results have been found before in a similar distance range [*Vidale and Earle*, 2000; *Koper et al.*, 2004; *Leyton and Koper*, 2007b]. In addition, we find that the duration of the ICS waves shrinks with increasing distance. This is consistent with the synthetic modeling of inner-core scattering assuming a single-scattering model [*Leyton and Koper*, 2007a], and the multiple scattering simulations using one of the best models (ε = 1.0%, a = 4.0 km) across a wide range of distances (Figure 11c).

[28] At smaller distances the growth of the ICS is flatter and more gradual. There is also a larger influence of crust and mantle scattering ("normal coda") at these distances because of the relatively large amplitude of the direct *PKiKP* phase. This is consistent with the previous observations that have found normal, monotonically decaying *PKiKP* coda when the parent *PKiKP* phase itself has significant amplitude [*Poupinet and Kennett*, 2004; *Koper et al.*, 2004; *Kawakatsu*, 2006; *Leyton and Koper*, 2007b], as well as the anticorrelation of the *PKiKP* phase and ICS waves observed in this study. Part of this phenomenon is also attributable to the fact that at smaller distances the steep ray angles of *PKiKP* make the ICS waves most sensitive to perturbations in density rather than velocity. Since density perturbations in the inner core are expected to be low (we use none in our modeling here), it is expected that the ratio of crust/mantle scattering to inner-core scattering in *PKiKP* coda waves will increase as distance decreases.

8. Conclusion

[29] Additional observations of ICS waves during the coda of *PKiKP* phase at LASA from a wide range of distance further confirm the existence of strong heterogeneities in the upper few hundred kilometers of the inner core with scale length of a few kilometers [*Vidale and Earle*, 2000; *Koper et al.*, 2004; *Leyton and Koper*, 2007b]. This conclusion is supported by the following lines of evidence:

[30] 1. The ICS waves have slowness similar to the *PKiKP* waves (Figure 3), indicating that they are scattered either at the inner-core boundary, or inside the inner core.

[31] 2. There is an apparent anticorrelation between the quality of the *PKiKP* and ICS waves (Figure 6). Most ICS waves are observed at distances of 45°–75°, where their parent *PKiKP* waves are nearly absent, suggesting that the ICS waves are transmitted into the inner core and then backscattered.

[32] 3. The majority of the ICS waves have spindle-shaped coda, with initial growth in amplitude with time followed by exponential decay (Figures 4 and 5). Recent analysis by *Leyton and Koper* [2007a] suggests that the spindle-shaped coda can only be generated by volumetric scattering in the uppermost portion of the inner core.

[33] 4. The durations of the coda and initial growth times shrink with increasing distances. This is consistent with the synthetic modeling of ICS waves assuming single-scattering inside the inner core [*Leyton and Koper*, 2007a] and the multiple scattering shown in Figure 11c.

[34] In addition, we found that most ICS waves are generated for raypaths sampling the Pacific Ocean and Asia, and relatively few observations are from the Atlantic Ocean. Although the SNR and number of events may play some role, our observation is roughly consistent with hemispheric patterns of the inner-core structure [e.g., *Niu and Wen*, 2001; *Leyton and Koper*, 2007b]. The average *Qc* values of ~600 in this study is similar to the average value of ~500 observed from a global data set of ICS waves [*Leyton and Koper*, 2007b]. The inferred heterogeneities with the length scale of kilometers in the uppermost inner core could be related to misalignments of crystals [*Bergman et al.*, 2002, 2005; *Bergman*, 2003], small-scale variations in orientation of anisotropy and attenuation [*Cormier and Li*, 2002], presence of partial melt [*Singh et al.*, 2000], and/or impurities [*Jephcoat and Olson*, 1987; *Lin et al.*, 2002]. Our results indicate that systematic analysis of ICS waves provides important constraints on the fine-scale heterogeneity of the inner core. Further constraints on the lateral variation in inner-core scattering strength are expected in the near future as data accumulates from some of the newer small and medium aperture arrays deployed in Central Asia and North Africa for nuclear monitoring purposes.

[35] **Acknowledgments.** We thank Paul Earle for making the catalog and waveforms of the LASA data available. The paper benefited from valuable comments by Vernon Cormier, the anonymous associate editor, and referee. This work is supported by NSF grant EAR99–02995 (JEV) and EAR0536438 (KP).

References

Bergman, M. I. (2003), Solidification of Earth's core, in *Earth*'s *Core: Dynamics, Structure, Rotation*, *Geodyn. Ser.*, vol. 31, edited by V. Dehant et al., pp. 105–127, AGU, Washington, D. C.

Bergman, M. I., D. M. Cole, and J. R. Jackson (2002), Preferred crystal orientations due to melt convection during solidification, *J. Geophys. Res.*, *107*(B9), 2201, doi:10.1029/2001JB000601.

Bergman, M. I., M. Macleod-Silberstein, M. Haskel, B. Chandler, and N. Akpan (2005), A laboratory model for solidification of Earth's core, *Phys. Earth Planet. Inter.*, *153*, 150–164, doi:10.1016/j.pepi.2005.03.016.

Cao, A., and B. Romanowicz (2004), Hemispherical transition of seismic attenuation at the top of the Earth's inner core, *Earth Planet. Sci. Lett.*, *228*, 243–253, doi:10.1016/j.epsl.2004.09.032.

Cormier, V. F. (2007), Texture of the uppermost inner core from forward- and back-scattered seismic waves, *Earth Planet. Sci. Lett.*, *258*, 442–453, doi:10.1016/j.epsl.2007.04.003.

Cormier, V. F., and X. Li (2002), Frequency-dependent attenuation in the inner core 2. A scattering and fabric interpretation, *J. Geophys. Res.*, *107*(B12), 2362, doi:10.1029/2002JB001796.

Creager, K. C. (1999), Large-scale variations in inner core anisotropy, *J. Geophys. Res.*, *104*, 23,127–23,139, doi:10.1029/1999JB900162.

Dziewonski, A. M., and D. L. Anderson (1981), Preliminary reference Earth model, *Phys. Earth Planet. Inter.*, *25*, 297–356, doi:10.1016/0031-9201(81)90046-7.

Earle, P. S., and P. M. Shearer (1998), Observations of high-frequency scattered energy associated with the core phase PKKP, *Geophys. Res. Lett.*, *25*, 405–408, doi:10.1029/97GL53365.

Engdahl, E. R., and C. P. Felix (1971), Nature of travel-time anomalies at LASA, *J. Geophys. Res.*, *76*, 2706–2715, doi:10.1029/JB076i011p02706.

Frankel, A., and R. W. Clayton (1986), Finite difference simulations of seismic scattering: Implications for the propagation of short-period seismic waves in the crust and models of crustal heterogeneity, *J. Geophys. Res.*, *91*, 6465–6489, doi:10.1029/JB091iB06p06465.

Frosch, R. A., and P. E. Green (1966), The concept of the large aperture seismic array, *Proc. R. Soc. London, Ser. A*, *290*, 368–384, doi:10.1098/rspa.1966.0056.

Hedlin, M. A. H., P. Earle, and H. Bolton (2000), Old seismic data yield new insights, *Eos Trans. AGU*, *81*(41), 469.

Hong, T. K., and R. S. Wu (2005), Scattering of elastic waves in geometrically anisotropic random media and its implication to sounding of heterogeneity in the Earth's deep interior, *Geophys. J. Int.*, *163*, 324–338, doi:10.1111/j.1365-246X.2005.02760.x.

Jephcoat, A., and P. Olson (1987), Is the inner core of the Earth pure iron?, *Nature*, *325*, 332–335, doi:10.1038/325332a0.

Kawakatsu, H. (2006), Sharp and seismically transparent inner core boundary region revealed by an entire network observation of near-vertical PKiKP, *Earth Planets Space*, *58*(7), 855–863.

Koper, K. D. (2005), The Generic Array Processing (GAP) software package, *Seismol. Res. Lett.*, *76*, 226.

Koper, K. D., J. M. Franks, and M. Dombrovskaya (2004), Evidence for small-scale heterogeneity in Earth's inner core from a global study of PKiKP coda waves, *Earth Planet. Sci. Lett.*, *228*, 227–241, doi:10.1016/j.epsl.2004.10.027.

Leyton, F., and K. D. Koper (2007a), Using PKiKP coda to determine inner core structure: 1. Synthesis of coda envelopes using single-scattering theories, *J. Geophys. Res.*, *112*, B05316, doi:10.1029/2006JB004369.

Leyton, F., and K. D. Koper (2007b), Using PKiKP coda to determine inner core structure: 2. Determination of QC, *J. Geophys. Res.*, *112*, B05317, doi:10.1029/2006JB004370.

Lin, J. F., D. L. Heinz, A. J. Campbell, J. M. Devine, and G. Shen (2002), Iron-silicon alloy in the Earth's core?, *Science*, *295*, 313–315, doi:10.1126/science.1066932.

Mitchell, B. J. (1995), Anelastic structure and evolution of the continental crust and upper mantle from seismic wave attenuation, *Rev. Geophys.*, *33*, 441–462, doi:10.1029/95RG02074.

Niu, F., and L. Wen (2001), Hemispherical variations in the seismic velocity at the top of the Earth's inner core, *Nature*, *410*, 1081–1084, doi:10.1038/35074073.

Poupinet, G., and B. L. N. Kennett (2004), On the observation of high frequency PKiKP and its coda in Australia, *Phys. Earth Planet. Inter.*, *146*, 497–511, doi:10.1016/j.pepi.2004.05.003.

Sato, H., and M. C. Fehler (1998), *Seismic Wave Propagation and Scattering in the Heterogeneous Earth*, AIP Press, New York.

Schimmel, M., and H. Paulssen (1997), Noise reduction and detection of weak, coherent signals through phase-weighted stacks, *Geophys. J. Int.*, *130*, 497–505, doi:10.1111/j.1365-246X.1997.tb05664.x.

Shearer, P. M., and P. S. Earle (2004), The global short-period wavefield modelled with a Monte Carlo seismic phonon method, *Geophys. J. Int.*, *158*, 1103–1117, doi:10.1111/j.1365-246X.2004.02378.x.

Shearer, P. M., and P. S. Earle (2008), Observing and modeling elastic scattering in the deep Earth, in *Earth Heterogeneity and Scattering Effects on Seismic Waves*, *Adv. Geophys.*, vol. 50, edited by H. Sato and M. Fehler, Elsevier, New York.

Singh, S. C., M. A. J. Taylor, and J. P. Montagner (2000), On the presence of liquid in the Earth's inner core, *Science*, *287*, 2471–2474, doi:10.1126/science.287.5462.2471.

Song, X. D. (2003), 3D structure and differential rotation of the inner core, in *Earth*'s *Core: Dynamics, Structure, Rotation*, *Geodyn. Ser.*, vol. 31, edited by V. Dehant et al., pp. 45–64, AGU, Washington, D. C.

Tromp, J. (2001), Inner-core anisotropy and rotation, *Annu. Rev. Earth Planet. Sci.*, *29*, 47–69, doi:10.1146/annurev.earth.29.1.47.

Vidale, J. E., and P. S. Earle (2000), Fine-scale heterogeneity in the Earth's inner core, *Nature*, *404*, 273–275, doi:10.1038/35005059.

Vidale, J. E., D. A. Dodge, and P. S. Earle (2000), Slow differential rotation of the Earth's inner core indicated by temporal changes in scattering, *Nature*, *405*, 445–448, doi:10.1038/35013039.

Wen, L., and F. Niu (2002), Seismic velocity and attenuation structures in the top of the Earth's inner core, *J. Geophys. Res.*, *107*(B11), 2273, doi:10.1029/2001JB000170.

K. D. Koper, Department of Earth and Atmospheric Sciences, Saint Louis University, St. Louis, MO 63103, USA.

F. Leyton, Departamento de Geofísica, Universidad de Chile, Blanco Encalada 2002, 1058 Santiago, Chile.

Z. Peng, School of Earth and Atmospheric Sciences, Georgia Institute of Technology, Atlanta, GA 30332, USA. (zhigang.peng@eas.gatech.edu)

P. Shearer, Institute of Geophysics and Planetary Physics, Scripps Institution of Oceanography, University of California, San Diego, La Jolla, CA 92093-0225, USA.

J. E. Vidale, Department of Earth and Space Sciences, University of Washington, Seattle, WA 98195, USA.